

Laser heated diamond cell system at the Advanced Photon Source for *in situ* x-ray measurements at high pressure and temperature

Guoyin Shen,^{a)} Mark L. Rivers, Yanbin Wang, and Stephen R. Sutton
Consortium for Advanced Radiation Sources, University of Chicago, Chicago, Illinois 60637

(Received 10 July 2000; accepted for publication 2 October 2000)

We describe a laser heated diamond anvil cell system at the GeoSoilEnviroCARS sector at the Advanced Photon Source. The system can be used for *in situ* x-ray measurements at simultaneously ultrahigh pressures (to >150 GPa) and ultrahigh temperatures (to >4000 K). Design goals of the laser heating system include generation of a large heating volume compared to the x-ray beam size, minimization of the sample temperature gradients both radially and axially in the diamond anvil cell, and maximization of heating stability. The system is based on double-sided laser heating technique and consists of two Nd:YLF lasers with one operating in TEM₀₀ mode and the other in TEM₀₁* mode, optics to heat the sample from both sides, and two spectroradiometric systems for temperature measurements on both sides. When combined with an x-ray microbeam (3–10 μm) technique, a temperature variation of less than 50 K can be achieved within an x-ray sampled region for longer than 10 min. The system has been used to obtain *in situ* structural data and high temperature equations of state on metals, oxides, and silicates to 3500 K and 160 GPa.

© 2001 American Institute of Physics. [DOI: 10.1063/1.1343867]

I. INTRODUCTION

As a unique method to reach ultrahigh static P – T conditions ($P > 100$ GPa, $T > 1500$ K), the laser heated diamond anvil cell (LHDAC) has been widely used for high P – T studies^{1–5} such as syntheses of high P – T phases,^{2,6} phase transition studies,^{7,8} high pressure melting,^{7,9,10} and P – V – T equations of state.^{11,12} Major advances have been made in the LHDAC technique in the last two decades in heating capability,^{4,13} temperature measurement,^{4,14} temperature control,^{15,16} and minimization of temperature gradients within the sampling region.^{17,18} The last is especially important for the application of this technique to x-ray measurements on a heated sample at high pressures. Recently the LHDAC has been combined with *in situ* x-ray diffraction at high P – T .^{5,12,19,20} The high brilliance of synchrotron radiation allows control of the x-ray beam to a size smaller than that of the laser heating spot, but still with enough photon flux to accurately measure x-ray diffraction and to conduct a variety of x-ray spectroscopy measurements.

There are several critical issues in LHDAC experiments with synchrotron radiation. (1) The heating spot must be much larger in size than the x-ray beam; (2) temperature gradients in both the radial and axial directions should be minimized to be less than other experimental uncertainties, e.g., diffraction accuracy; (3) a steady temperature is required for the x-ray measurement; (4) the micro-x-ray beam should be well collimated to avoid contamination from strong scattering by surrounding materials (e.g., gasket); and (5) the pressure and temperature of the sampling area should be well controlled and determined.

Here we report a new LHDAC facility at the

GeoSoilEnviroCARS sector at the Advanced Photon Source (APS). The design goals of our system are to

- (1) provide a sufficiently large heating spot relative to the x-ray beam,
- (2) minimize sample temperature gradients both radially and axially,
- (3) control and measure temperature precisely and easily,
- (4) perform *in situ* x-ray measurements at controlled high P – T conditions.

II. LASERS

Criteria for choosing a heating laser include the total power, beam divergence, stability, wavelength, and power distribution (mode structure). Diamond has the highest thermal conductivity among known materials. Lasers should have sufficiently high power with low divergence to be able to focus down to a desired size and to have enough power density to heat samples at high pressure between the two diamond anvils. Lasers with high power stability and beam pointing stability are essential for producing a heating spot at steady temperature and at a constant position. The choice of laser wavelength depends on the materials to be heated. Nd:YAG and Nd:YLF lasers with 1.064 and 1.053 μm wavelengths, respectively, are often used for opaque materials, while CO₂ lasers (wavelength of 10.64 μm) are applied for transparent samples, such as oxides and silicates. The fundamental mode (TEM₀₀) of the laser is often used^{4,21,22} for LHDAC because it provides a laser beam with low divergence and high stability. The drawback of using a TEM₀₀ mode laser is the temperature gradient in the heated area resulting from the Gaussian intensity distribution. Multimode lasers¹⁷ can provide a relatively flat top in the intensity pro-

^{a)}Electronic mail: shen@cars.uchicago.edu

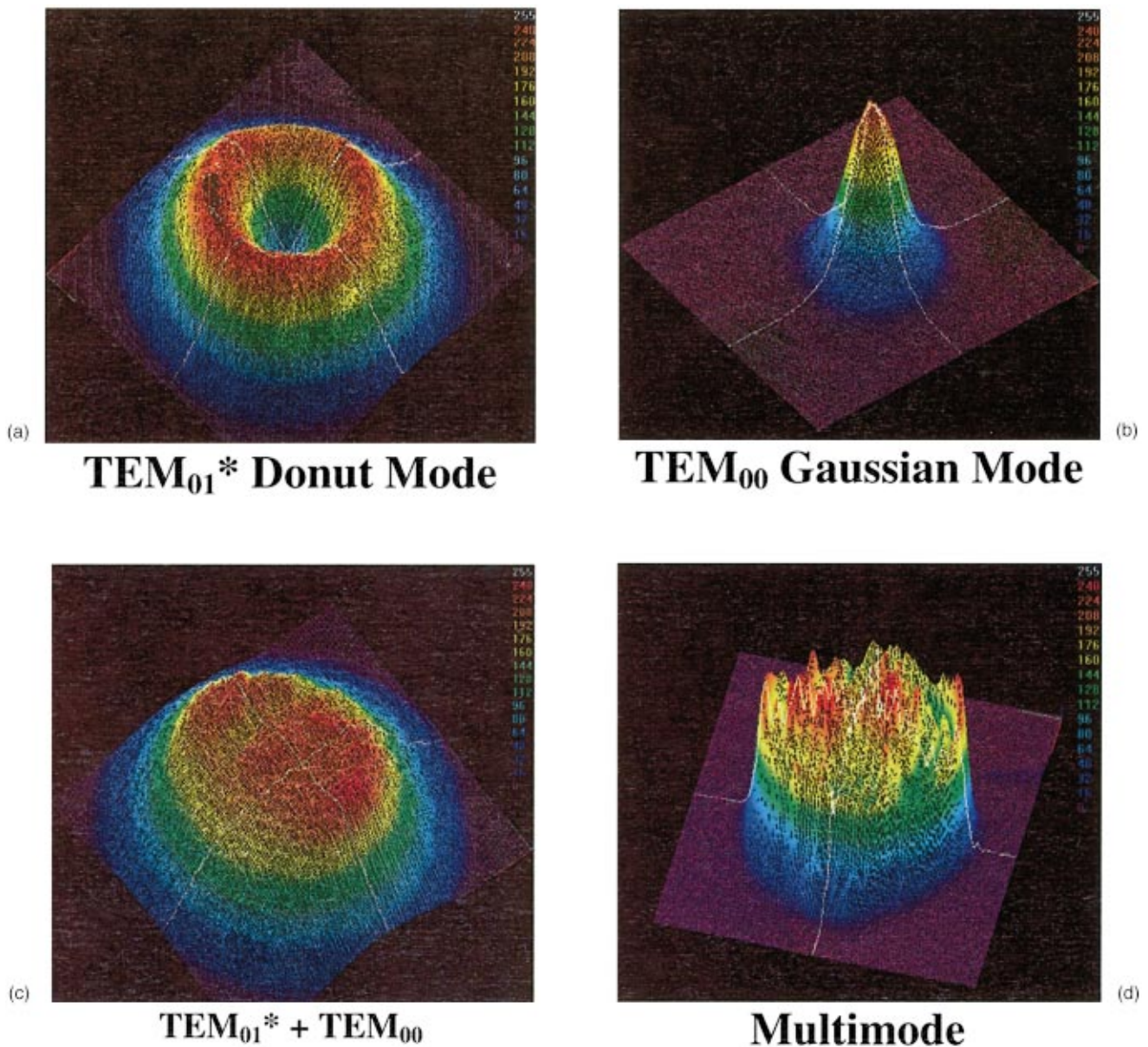


FIG. 1. (Color) Beam profiles in two dimensions of Nd:YLF lasers measured by a laser beam analyzer (Spiricon, LBA-300PC). The vertical axis is the power intensity. (a) TEM₀₁* (donut) mode; (b) TEM₀₀ Gaussian mode; (c) TEM₀₁*+TEM₀₀; (d) multimode. Note that a flat top (c) in power intensity can be constructed by combining two lasers (a) and (b), compared to the multimode laser which has at least 20% power fluctuation at the top.

file. However, compared to single mode lasers, multimode lasers have a relatively large beam divergence, power instability, and beam pointing instability.

We have developed a laser heating system consisting of two Nd:YLF lasers with one operating in the TEM₀₁* mode [donut mode, Fig. 1(a)] and the other in the TEM₀₀ mode [Gaussian mode, Fig. 1(b)] with maximum power of 65 and 50 W, respectively. The combined beam of the two Nd:YLF lasers provides a total power of 105 W, comparable to that of multimode lasers and more than three times larger than that of generally used TEM₀₀YAG (or YLF) lasers. The YLF lasers provide sufficient collimation for our focusing requirements and the power stability and especially the pointing stability are superior to those of YAG lasers. More importantly, the two-laser system allows us to *construct* a desired beam profile and, as a consequence, a laser heating spot with

a minimum radial temperature gradient in the center area ($\sim 20 \mu\text{m}$ in diameter) is achieved. This tunability is crucial because the power mixing ratio of the two lasers depends strongly on the material being heated. Figure 1 shows the intensity profiles measured from these two lasers. By adjusting the power ratios of two lasers, a flat top in power intensity can be reached [Fig. 1(c)].

III. OPTICS

A. Heating optics

A schematic diagram of the optical system is shown in Fig. 2. The guiding optics include power regulators, laser power controller, combining optics, laser power detector, beam splitter, and focusing optics. The two YLF lasers operate in continuous wave (cw) mode, with the TEM₀₀ mode

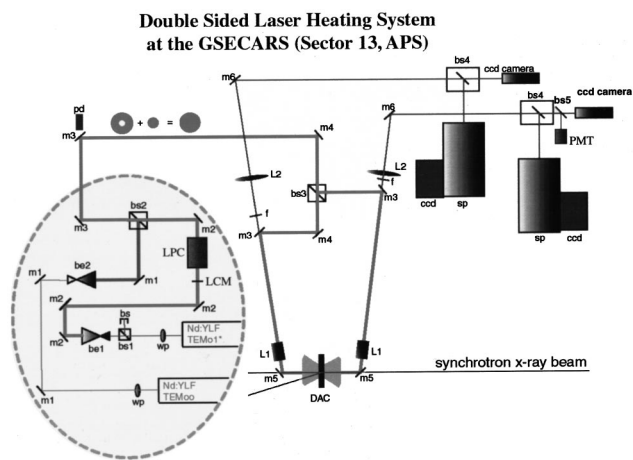


FIG. 2. Schematics of the double-sided laser heating system at the GeoSoilEnviroCARS sector at the APS. be1, be2: Zoom beam expander (Special Optics); bs1, bs2: polarized cube beamsplitter (Newport); bs3: non-polarized 50/50 cube beamsplitter (Newport); bs4: 50/50 neutral beamsplitter (Optics for Research); bs5: 90/10 pellicle beamsplitter (Newport); ccd camera: Panasonic CCD camera, WV CP-612; ccd: CCD detector (TE-1100 PB, Princeton Instruments) (Roper Scientific); DAC: symmetrical diamond anvil cell (Ref. 18); L1: apochromatic objective lens, 60 mm focal length (US Laser); L2: achromatic lens, 1000 mm focal length (Oriel); LPC: laser power controller (Cambridge Research Instruments); m1: dichroic mirror, reflecting (>99%) vertical polarized laser beam at 1053 nm (Photonics); m2: dichroic mirror, reflecting (>99%) laser beam at 1053 nm (Photonics); m3, m5: dichroic mirror, reflecting (>99%) laser beam at 1053 nm and transmitting visible light (>90%) (Optics for Research); m4: dichroic mirror, reflecting (>99%) laser beam at 1053 nm and visible light (>40%) (New Focus); m6: beryllium or glassy carbon mirror coated with silver; m7: Al coated mirror (Newport); nf: notch filter (HNPF-1064.0-2.0, Kaiser Optical System); pd: photodiode for monitoring the laser power; PMT: photomultiplier tube (Hamamatsu); sp: spectrograph (Holospec $f/2.2$, Kaiser); wp: wave plate (Newport).

laser vertically polarized and the TEM₀₁* laser horizontally polarized. The polarized beam makes it possible to regulate laser power by changing the polarization direction. The laser power regulator consists of a wave plate (wp), a cube beam splitter (bs1), and a beam stop (bs). The two laser beams with different polarization are combined into one by a cube beamsplitter (bs2). Before combining the two lasers, a laser power control system (Cambridge Research Inc.) is installed in the path of the TEM₀₁* laser. Two photodiodes (pd) behind mirrors monitor the output power of each laser. The combined beam is steered by two mirrors and is split into two by a 50/50 nonpolarizing beamsplitter (bs3). Each branch is then reflected by a dichroic mirror (m5) which reflects >99.9% of the 1.053 μm laser light and transmits >90% of the visible portion of the spectrum. An apochromatic objective lens (L1, $f = 60$ mm) is used to focus the beam onto the sample. A beryllium or glassy carbon mirror (m6) coated with silver is employed between the objective lens and the sample. This mirror is used to guide the laser beam and receive the sample image and thermal radiation signals, while allowing x rays to pass through for various x-ray measurements. More discussion of the mirror (m6) is given below in Sec. VI.

B. Optics for temperature measurement

The sample image and its thermal radiation are collected by the laser-focusing apochromat (L1) and focused onto a

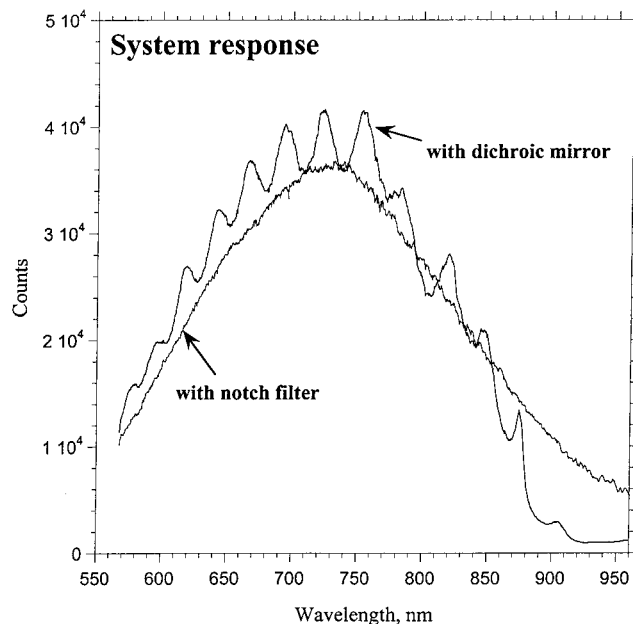


FIG. 3. System responses from a standard lamp. If m5 in Fig. 2 is replaced by a notch filter, a smooth system response can be obtained. However, the notch filter has a limited reflectivity of ~95% at the laser wavelength. Damage may occur when high power density laser is used.

charge coupled device (CCD) with an achromatic lens (L2, $f = 1000$ mm). L1 and L2 provide magnification of about 17×. A 50/50 beamsplitter (bs4) is used, with one transmitted branch for viewing by a CCD camera and the reflected branch for spectroscopic measurement (sp). Use of the reflected branch avoids introducing chromatic aberration. Optics in the whole path for temperature measurement include a mirror (m6), an apochromatic lens (L1), a dichroic mirror (m5), a notch filter (nf), and a 50/50 neutral density beamsplitter.

Figure 3 shows a typical system response of the optics. The dichroic mirror reflects the laser beam and transmits the thermal radiation signal. This mirror introduces some interference color in the spectra collected (Fig. 3). By replacing the dichroic mirror with a notch filter (Kaiser Optical System), the interference color can be minimized (Fig. 3). The notch filter has excellent transmission (>95%) in the visible and up to a wavelength of 900 nm, but the reflectivity at the laser wavelength (1.053 μm) is only about 95%, compared to >99% reflectivity for the dichroic mirror. When applied with full laser power, notch filters may be damaged.

The path from the dichroic mirror to the sample position is coaxially aligned to the heating laser path. If the incident beam is normal to the diamond anvil surface, this coaxial arrangement ensures that the thermal radiation signal is collected from the laser heating spot even though the image position (as well as the heating spot) is changed by adjusting mirror m6. The combined coaxial path simplifies the alignment procedures when the system is coupled to x-ray diffraction or other measurements.

C. Imaging spectroscopy

The spectroradiometric system consists of a thermoelectrically cooled CCD detector (Princeton Instruments, TE/

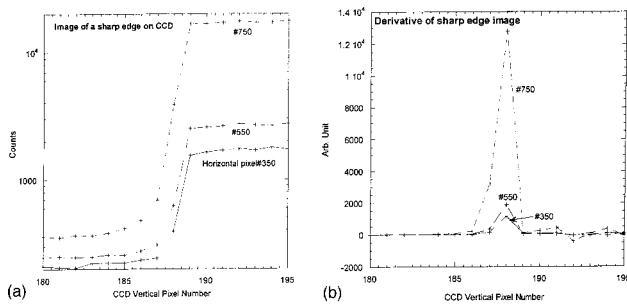


FIG. 4. (a) Images of a sharp edge on the CCD detector. A $10\ \mu\text{m}$ thick sharp edge was placed at the middle of the entrance slit. White light from tungsten lamp was backilluminated to the slit. (b) The derivative of (a). Pixel Nos. 350 and 750 correspond to 681 and 824 nm in wavelength, respectively. This closely covers the wavelength range (670–830 nm) normally used in temperature calculation.

CCD-1100PB) and a Kaiser spectrograph (HoloSpec, $f/2.2_{\text{vis}}$). HFG-750 grating is used, and covers the wavelength range of 550–920 nm with a central wavelength at 750 nm. It gives a wavelength resolution of 1.1 nm with an $80\ \mu\text{m}$ entrance slit. The main advantage of the Kaiser spectrograph is its excellent imaging quality, i.e., superior spatial resolution along the direction perpendicular to wavelength dispersion. Because a transmission grating is used, the Kaiser holospec spectrograph gives superior spatial resolution compared with a reflection grating.²³ To check the imaging quality, a $10\ \mu\text{m}$ thick gold foil was attached to the middle of the entrance slit. The sharp edge of the gold foil was backilluminated with a white light source and recorded on the CCD (Fig. 4). The derivative of the recorded sharp edge [Fig. 4(b)] shows that the full width at half maximum (FWHM) is less than 1.5 pixels in the spectrum range of interest from 681 to 824 nm, reaching the resolution limit of the CCD. The pixel size of the CCD detector for thermal radiation collection is $27 \times 27\ \mu\text{m}^2$. When the detector is replaced by a CCD with a pixel size of $12 \times 12\ \mu\text{m}^2$ the FWHM in the derivative plot is still less than 1.5 pixels, indicating that the spatial resolution of the spectrograph along the direction perpendicular to the wavelength dispersion is better than the pixel size ($27\ \mu\text{m}$).

Another factor to be considered is the curvature in the slit image. The image of a straight slit through a spectrograph using a plane grating will result in a curved image, in most cases parabolic, due to the fact that rays from different positions along the slit are incident on the grating with varying amounts of obliqueness. Because of the short focal length of the HoloSpec spectrograph, the amount of obliqueness for rays at both ends of the slit is larger than for spectrographs with long focal lengths. Therefore, we use only the middle 60 pixels for temperature measurement. The CCD chip has 330×1100 pixels. For rays covering the center 1.6 mm of the slit (corresponding to 60 pixels on the CCD), displacement from the center ray is less than $12\ \mu\text{m}$. Binning in this region can be made with no degradation in wavelength resolution for the CCD camera.

The imaging spectrometer allows us to measure simultaneously all points on a linear temperature profile across a laser heated spot, as opposed to measurement of only a small point, or an “average” temperature of a laser heated spot. As

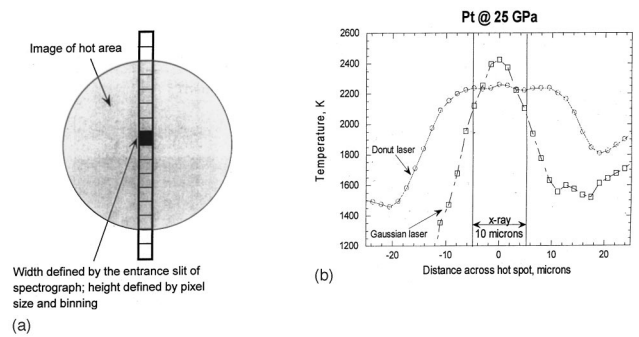


FIG. 5. (a) Image of a hot spot on the entrance slit. A temperature profile in the vertical direction can be obtained for each measurement. (b) Temperature profiles with a TEM_{00} laser and a TEM_{01}^* laser for platinum at 25 GPa in a DAC. NaCl was used as an insulating layers on both sides.

indicated in Fig. 5(a), the entrance slit of the spectrograph is used to select a thin strip traversing the laser spot. Through the spectrograph, this linear strip is imaged onto the $60(\text{rows}) \times 1100(\text{columns})$ pixels on CCD. Each row corresponds to a point of the strip with its thermal radiation wavelength spreading over each column. The chosen entrance slits measures $80\ \mu\text{m}$ which is equivalent to about $4.7\ \mu\text{m}$ on the sample. The center 60 pixels cover about $95\ \mu\text{m}$ across a hot spot. The pixel binning can be adjusted with software and the typical binning number is 3, which is equivalent to the size of the entrance slit. Thus a temperature profile across the hot spot of about $95\ \mu\text{m}$ in 20 binned pixels is measured [Fig. 5(b)].

IV. TEMPERATURE MEASUREMENT

A. Spectral radiometry

The accuracy and precision of temperature measurements in the laser heated diamond anvil cell have been much improved in the past with the use of spectral radiometry.^{3,17,24,25} This method is also adopted in our system. Temperatures are determined by fitting the thermal radiation spectrum between 670 and 830 nm to the Planck radiation function:

$$I_{\lambda} = c_1 \varepsilon(\lambda) \lambda^{-5} / [\exp(c_2 / \lambda T) - 1], \quad (1)$$

where I_{λ} is spectral intensity, ε emissivity, λ wavelength, T temperature, and $c_1 = 2\pi h c^2 = 3.7418 \times 10^{-16}\ \text{W m}^2$, $c_2 = hc/k = 0.014388\ \text{mK}$. The system response is calibrated by a tungsten ribbon lamp (OL550, Optronic Laboratories) with known radiance, according to National Institute for Standards and Technology (NIST) standards. Figure 6 shows a radiation spectrum after normalization to the system response and its fit to the Planck radiation function.

B. Precision and accuracy

Temperature measurements by spectral radiometry have been validated by many authors.^{4,15,17} Our system has been verified by the following four methods. (1) The second known radiation point (at 2000 K, provided by manufacturer) of the standard lamp. The radiation of the second point is

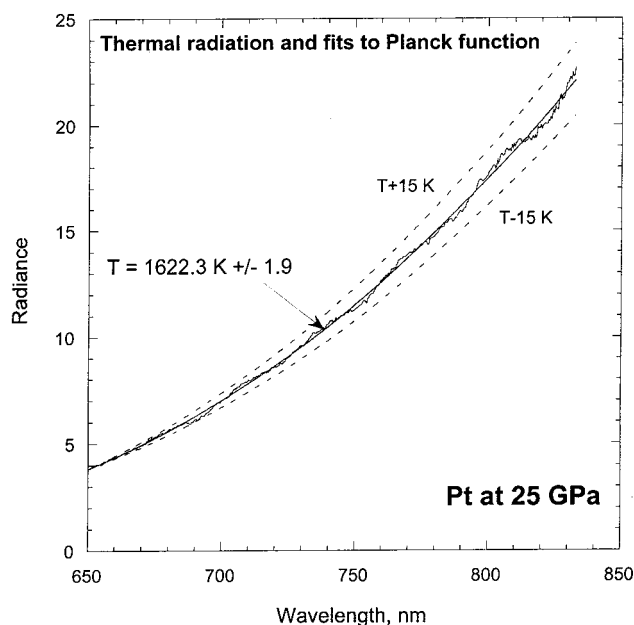


FIG. 6. Example of thermal radiation normalized to the system response and the fit (solid line) to Planck radiation. The fitting error is shown. To show the precision of this method, dashed lines with temperatures above and below 15 K of 1622.3 K are plotted.

always measured during each calibration. We obtained 1994 ± 5 K in our calibration measurements over three years. (2) Visual observation of melting of a Pt foil at ambient pressure with laser heating. Three measurements gave a melting temperature of 2060 ± 30 K for Pt, close to the literature value of 2045 K. (3) Double-sided laser heating on a Pt–Pt/Rd thermocouple with a junction bead of about $40 \mu\text{m}$ in diameter. Temperatures were measured both by spectral radiometry and the thermocouple. Temperatures from the spectral radiometry are systematically ~ 95 K higher than those from the thermocouple emf (Fig. 7). The low temperature read by the thermocouple may result from the fact that the laser heating spot ($\sim 30 \mu\text{m}$ in diameter) is slightly smaller than the junction bead. Note that the standard deviation of the temperature difference is 15 K over the temperature range of 1300–1600 K covered, indicating the precision of the temperature measurement by the spectral radiometry system. (4) A Pt–Pt/Rh thermocouple in a resistance heating furnace. Heat was applied with the furnace. Again, temperatures were recorded by both spectroradiometry and thermocouple emf (Fig. 7). It is found that temperatures measured by spectral radiometry are about 51 ± 8 K higher than those measured by thermocouple emf over the temperature range (1000–1500 K) covered. The high temperature measured by spectroradiometry could partly arise from radiation from the furnace walls that were hotter than the center where the thermocouple was located. In addition, the calculated spectroradiometry temperature will be reduced when the wavelength dependence of emissivity is considered in fitting to the Planck radiation. From the available data for Pt,²⁶ this modification will be ~ 30 K in this temperature range. Both of the factors will reduce the difference between the two methods. Over the temperature interval (380 K), the difference has a standard deviation of 8 K, indicating the precision of tem-

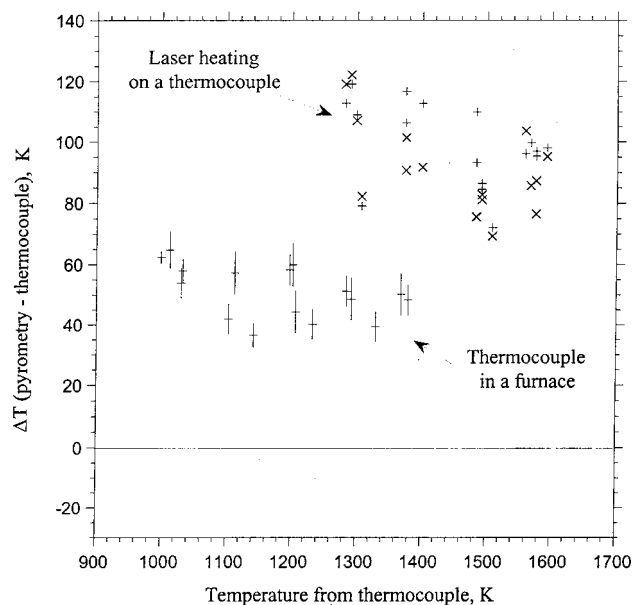


FIG. 7. Temperatures at a thermocouple junction measured by spectral radiometry and thermocouple emf. The differences in temperature between two methods are plotted vs the temperatures from the thermocouple. Data obtained from two experiments are shown. (1) Double-sided laser heat with a heating spot of $\sim 30 \mu\text{m}$ was applied on a junction $\sim 40 \mu\text{m}$ in diameter. (2) The thermocouple was placed at the center in a furnace.

perature measurement by the spectral radiometry in our system.

The statistical errors in fitting to Planck radiation are demonstrated in Fig. 6. Typical standard deviations are only a few degrees. For example, the dashed lines in Fig. 6 show the fittings for temperatures above and below by only 15 K. Clearly, these lines are already out of the data set region.

The accuracy of temperature measurement using spectral radiometry in the diamond anvil cell is mainly affected by the wavelength dependence of emissivity [Eq. (1)] and system's optical aberration. The effect of wavelength dependent emissivity can be considered in temperature calculations with known emissivity data.^{4,22} However, such data show large scatter in the literature even at ambient conditions; no data are available at high P – T . Currently most investigators assume constant emissivity over the wavelength range being fit to the Planck's radiation function. From known emissivity data at 1 atm, e.g., for tungsten, different wavelength dependences of emissivity at 2000 and 3000 K can change the calculated temperature by over 75 and 200 K, respectively. The lack of wavelength dependence information on emissivity at high P – T limits the accuracy of temperature measurements in the laser heated diamond anvil cell, especially at temperatures over 3000 K. By reducing the fitting wavelength range, this error from emissivity can be reduced. However, too small a wavelength range may introduce errors in calculated temperature from some nonlinear portion of the system response (see, for example, Fig. 6). A minimum wavelength range of 50 nm is required in our system. We normally use a wavelength range of 670–830 nm, covering 160 nm.

Another major source of error in the temperature measurement arises from the temperature gradient in a small hot

spot, as was pointed out by Boehler and Chopelas.¹⁶ High accuracy in temperature measurements critically depends on two strongly related factors: minimization of the chromatic aberration of optical systems and temperature uniformity of a heating area. As a diamond window is always involved in DAC experiments, the system cannot be dispersion free. Therefore, the latter is very important and is the object of our development. If the heating area is uniform, the uncertainty due to chromatic aberration can be eliminated by calibration.¹⁷ So far most verifications^{4,15,17} for temperature measurement were made with a relatively uniform hot object. No verification has been done for a small hot spot where temperature gradients exist. It seems difficult to locate standards with known temperature gradients comparable in degree and size with the laser heating spot. Without such a calibration, little is known of the true values of a temperature profile obtained with an existing temperature gradient. On the other hand, by establishing a uniform heating region, temperature can be determined accurately even in the presence of a small chromatic aberration. Our system collects the thermal radiation from an area $4.5 \mu\text{m}$ across. An area of $>10 \mu\text{m}$ in diameter with a minimum temperature gradient can be considered a uniform temperature region. It should be emphasized that the chromatic aberration becomes a large source of error only when a large temperature gradients exist. Therefore, our efforts in minimizing temperature gradients in the laser heating spot are not only for establishing a large heating volume, but also for minimizing the chromatic aberration effect, and thus improving the T measurement accuracy.

The chromatic effect of our system was tested by placing a $25 \mu\text{m}$ pinhole at the sample position. The pinhole was back illuminated by a neon lamp, and the images of neon lines at 659.8 and 837.5 nm were recorded by the imaging spectrograph (Fig. 8). The “focus” position is determined by the visible light. We observed that the sharp image of the pinhole at 837.5 nm was found $10 \mu\text{m}$ from the focus position, indicating the magnitude of the chromatic aberration of our system. To check the effect on temperature arising from this aberration, temperatures from a laser heated spot were measured at three positions: the focus position and $20 \mu\text{m}$ in front and in back of it. The resulting temperatures at the center portion of the hot spot varied within 10 K at these three positions.

C. Radial and axial temperature gradients

A large heating spot is desired with minimal temperature gradients at the center part and steep gradients at the edge. To achieve such radial temperature distribution, the system should have sufficiently high laser power, an optimal power distribution of the laser beam, a homogeneous sample which strongly absorbs the laser beam, and a sample well insulated by low thermal conduction materials from diamond anvils which are essentially the heat sinks.

As shown in Fig. 1, our high power laser system allows us to construct a laser beam with the desired power distribution. The TEM₀₀ laser provides a heating spot with a Gaussian temperature profile, while TEM₀₁^{*} (the donut) laser gives

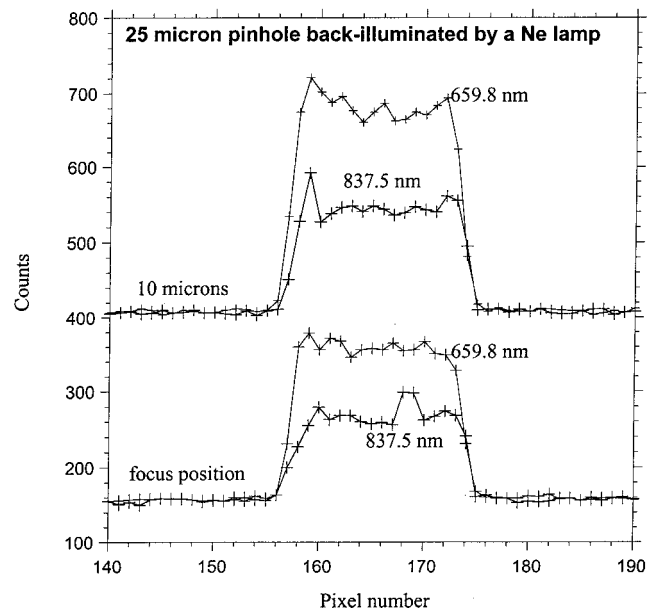


FIG. 8. Images of a $25 \mu\text{m}$ pinhole on a CCD detector at different wavelengths. The pinhole was placed at the sample position and backilluminated by a neon lamp. Images of neon lines at 659.8 and 837.5 nm are plotted which covers the wavelength range for temperature measurement. “Focus position” means a focused position determined by visible light. The image of 837.5 nm is not as sharp as that of 659.8 nm at the focus position. The sharp image of 837.5 nm was obtained when the position was changed $10 \mu\text{m}$.

a relatively flat top temperature distribution [Fig. 5(b)]. When the sample has high thermal conductivity (e.g., Pt metal), the donut laser alone often provides a favorable flat top temperature distribution [Fig. 5(b)]. For samples such as silicate perovskite, a shallow dip can be often seen in the temperature profile with the donut laser heating only (Fig. 9). In that case, a small portion of TEM₀₀ laser can be applied to obtain a more even temperature distribution. Determining the right power level of the TEM₀₀ laser is not an easy task. It depends on sample properties and on the loading configuration of each cell. Currently we gradually increase the power (TEM₀₀) until the desired temperature profile is reached. Because heating is interaction between a laser beam and the absorbing material, sample configuration is equally important in achieving the desired temperature profiles. The optimal power distribution of the laser beam is just the first step. The actual temperature distribution will strongly depend on the sample homogeneity and the use of insulating layers.

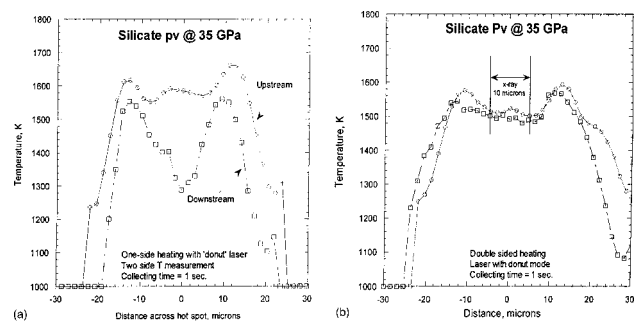


FIG. 9. Temperature profiles measured of both sides of a silicate perovskite sample at 35 GPa. (a) Single-sided heating with the TEM₀₁^{*} laser; (b) double-sided heating with the TEM₀₁^{*} laser.

Significant efforts have been made in sample preparation to have T profiles like those in Figs. 5 and 9.

The diamond anvils act as a heat sink and provide the low temperature boundary condition. The most severe temperature gradient in a sample exists along the path of the laser beam (the axial gradient). The double-sided laser heating^{17,18,27} minimizes the axial temperature gradient in the sample. This is an important step for *in situ* x-ray measurement with the LHDAC. As shown in Fig. 9(a), temperatures can differ by a few hundred degrees over an $\sim 5 \mu\text{m}$ thick sample with the single-sided heating method. On the same sample with the double-sided heating technique, the axial gradient is reduced to within 30 K at the sampling region [Fig. 9(b)].

Insulating layers play an important role in heating efficiency and temperature gradients. A good insulating material (e.g., argon, NaCl, MgO), should have low thermal conductivity and chemical inertness. Thicker insulating layers result in higher heating efficiency, larger heating area, and smaller temperature gradients both radially and axially. Efforts to increase the thickness of insulating layers have been made by introducing diamond powder gaskets.²⁸ These are far superior to conventional metal gaskets. For double-sided heating, efforts should be made to ensure that the layers at both sides are equal in thickness and evenly distributed.

V. TEMPERATURE CONTROL

A. Laser power control

Our YLF:Nd lasers have power instability of less than 1% peak to peak. A plot of the laser power as a function of time shows an instability frequency of 0.1 Hz, the same as that of the primary cooling water of the laser system, implying that the instability arises from the temperature instability in the laser chambers. The frequency domain after Fourier transformation showed no particular instability modes at high frequencies.

As can be seen from Fig. 2, a power regulator is introduced at the output of both TEM₀₁^{*} and TEM₀₀ lasers. The wave plate is mounted on a rotary motor that is remotely controlled by a picomotor driver (New Focus Inc.). The regulator allows one to fix the lamp current of the laser at the working point recommended by the manufacturer, and reaches maximum power and pointing stability. The regulated power can be monitored by two photodiodes (pd in Fig. 2) for both lasers. For the TEM₀₁^{*} laser, we installed a laser power controller (LPC). The LPC is similar to the one first introduced by Heinz *et al.*¹⁵ It consists of a liquid crystal, a cube beamsplitter (bs1), a 90/10 beamsplitter (bs2), a photodiode (pd), and an electronics control unit (Fig. 10). The laser polarization is changed by passing the beam through a birefringent liquid crystal wave plate. The beam is then attenuated by rejecting a portion of the beam by a cube beamsplitter (bs1). The birefringence of the liquid crystal and the attenuation are proportional to a voltage applied to the liquid crystal by the control unit.²⁹

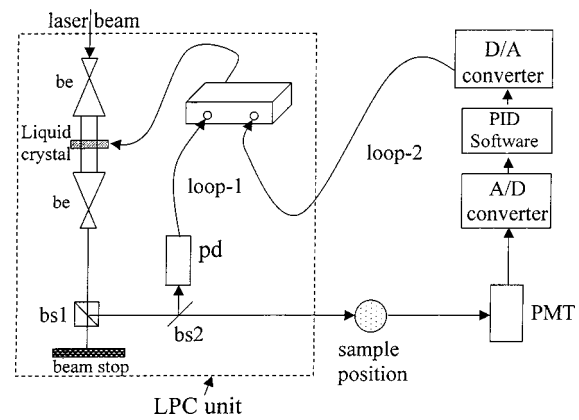


FIG. 10. Schematic of the laser power controller and the feedback loops. Loop 1: liquid crystal>bs1>bs2>pd>control unit>liquid crystal; loop 2: liquid crystal>bs1>sample>PMT>A/D converter>PID software>D/A converter>control unit>liquid crystal. be: Beam expander (6 \times , Optics for Research); bs1: polarized beamsplitter; bs2: 90/10 beamsplitter; pd: photodiode; PMT: photomultiplier tube; A/D: analog to digital converter (Acromag IP-330); PID software: fast running software (10 Hz); D/A: digital to analog converter (Systran DAC-128 V).

B. Feedback system

There are two feedback loops in the system (Fig. 10). One loop is from the photodiode monitoring the laser power (loop 1); the other is from the photomultiplier tube (PMT) monitoring the thermal radiation from the laser heated sample (loop 2). Loop 1 is actually a built-in feature of the LPC at constant power mode. Loop 2 is designed for stabilizing temperatures.

The TEM₀₁^{*} laser is used as the primary heating laser, while the TEM₀₀ laser is used for gaining power and/or improving temperature uniformity. Typically the power level of the TEM₀₀ laser in use is much less than that of the TEM₀₁^{*} laser. Therefore, the TEM₀₁^{*} laser power is used for the feedback system. The detector for feedback loop 2 is a PMT (Hamamatsu). A portion of the thermal radiation emitted from a heated sample from only one side is reflected by beamsplitter (sp5 in Fig. 2) to the PMT. An aperture 250 μm in diameter is placed in front of the PMT, which selects a region $\sim 15 \mu\text{m}$ in diameter at the laser heated spot. Instead of using a preamplifier for conditioning the PMT, we use fast software running on a VME crate. The enhanced proportional integral derivative (EPID) record allows flexible and fast feedback under our EPICS control system. The PMT signal is fed to an Acromag IP-330 analog to digital (A/D) converter for input and a Systran 128 V digital to analog converter for output. The EPID record runs on a largely dedicated CPU up to 10 kHz feedback rate. Output from the digital to analog converter is connected to modulation input of the LPC, and laser power is modulated through the liquid crystal to stabilize the thermal radiation. According to the Stephan-Boltzmann relation, $I = \epsilon\sigma T^4$, where ϵ is emissivity, and σ is the Stephan-Boltzmann constant, thermal radiation is a sensitive metric of temperature stability because it varies with the fourth power of temperature.

Figure 11 shows the thermal radiation with the set points and read back values, and temperatures measured from both sides. Temperatures can be stabilized for minutes to hours

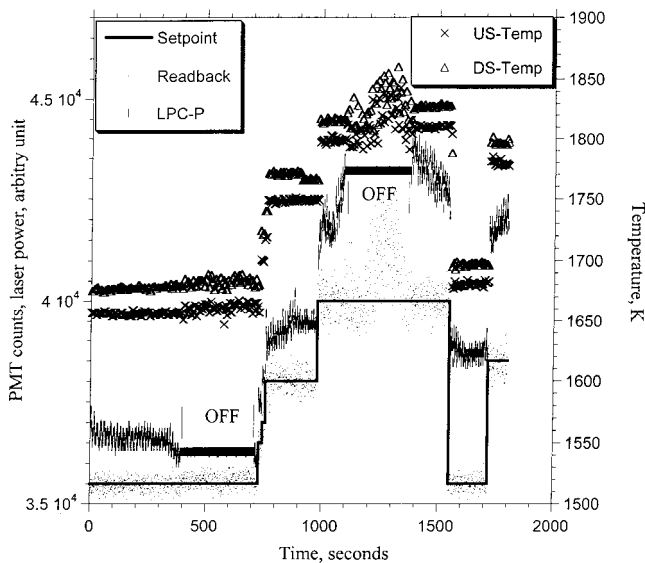


FIG. 11. Performance of a feedback system on a Pt foil. The set points (solid lines) and read back values (dots) for thermal radiation are plotted vs time together with the laser power (LPC-P, vertical bars) and temperatures measured from both sides (crosses for upstream temperatures and triangles for downstream). “OFF” denotes that feedback loop 2 was turned off and that loop 1 was being used, and is providing constant laser power. With feedback loop 2, a standard deviation of 1.8 K was reached in the first 6 min.

and can be controlled by simply changing the set point value through software. The relationship between the set point value and the temperature depends strongly on the sample properties and its configuration (e.g., absorbance, thickness of insulation layers). It is not possible to establish a general calibration between these two parameters. However, by viewing a live plot of the data in Fig. 10 during an experiment, one can quickly establish an empirical relationship. Therefore, temperatures can be easily set to the desired levels, and small changes in temperature become possible.

The feedback “off” in Fig. 11 means that the system is operating with only feedback loop 1, i.e., the laser power is being stabilized by the LPC. As shown, temperature fluctuation with loop 1 is larger than that with loop 2. For example, at temperatures around 1800 K the T fluctuation is ~ 80 and ~ 10 K with loop 1 and the loop 2, respectively. Thus the feedback from thermal radiation is superior to that which only monitors laser power.

VI. IN SITU X-RAY MEASUREMENTS AT HIGH P – T

A. Alignment

Proper alignment is crucial for accurate measurements, with all heating laser beams, thermal radiation paths, incident x-ray beams, and characterizing systems aligned to the sample position within a few microns. For practical applications, we mention two major aspects. One is the coaxial arrangement of the laser beam and the thermal radiation path. The other is the optical visibility of the x-ray beam. The coaxial path is established from the point of mirror m5 (Fig. 2) to the sample position for the laser beam and the path of thermal radiation. With the coaxial optics, it is possible to adjust the heated location using mirror m6 in Fig. 2 without

disturbing the internal alignment between the laser beam and the collected thermal radiation. In other words, temperature is always measured from the heating spot even though the heated spot moves as one adjusts mirror m6. This adjustment allows us to quickly align the laser heating system to the x-ray beam position. With the bright APS undulator beam, the luminescence of the sample or pressure medium is often visible using the sensitive CCD camera. For a clear image of the x-ray beam, diamond anvils of low fluorescence are required. The optically visible x-ray image can then be used for alignment to the laser heating system.

A typical alignment procedure for the system is as follows. The rotation center of the two circle diffractometer³⁰ is first aligned with the slit-defined (or focusing mirror-defined) incident x-ray beam. This center is then used as the reference point for all optics alignment including the two spectral radiometry systems for temperature measurement and the two heating laser beams (Fig. 2). This aligns the system for samples without the DAC. For DAC samples, first we need to set the DAC sample at the position for x-ray measurements. The DAC sample position is generally required to be at the rotation center. This can be done by using the x-ray beam or an additional fixed microscope. After fixing the DAC position, the focus of L1 (Fig. 2) can be adjusted to get the image of the DAC sample to compensate for the refractive index of the diamond window. Because the diamond window is not perfectly normal to the optical path, some fine-tuning is always needed. Now the critical reference is to know the x-ray beam position through the laser heating viewing system, CCD camera in Fig. 2. Fortunately, the x-ray induced luminescence of the sample or medium is often visible with the sensitive CCD camera. Since the relative positions of the CCD camera and the spectrometer (see Fig. 2) are fixed, we can take the point for temperature measurement (the spectrometer position) as a reference by making a crossmark on the screen. Then the visible x-ray image is aligned to the crossmark by adjusting mirror m6 in Fig. 2. The coaxial optics arrangement ensures that the crossmark is the laser heating spot as well as the region from which the thermal radiation is collected. Thus, the x-ray beam, heating spot, and the temperature measurement region are all aligned. If the x-ray luminescence is not seen, an x-ray marker (e.g., a tungsten grain $< 5 \mu\text{m}$) needs to be loaded with the sample and this marker should be optically visible. The x-ray position can then be determined by scanning the marker^{5,18} and aligned optically by mirror m6. As described above, adjustment of mirror m6 does not affect the internal alignment between the laser heating spot and the point for temperature measurement. These mirrors (m6) are remotely controlled by motors which provide easy and fast alignment with typical accuracy of $2\text{--}3 \mu\text{m}$.

B. Microbeam

From measured temperature profiles (Figs. 5 and 8), the system provides a laser heating spot $15\text{--}30 \mu\text{m}$ in diameter at the top 90% temperature level. At ultrahigh pressures, the spot size may reduce to $10\text{--}20 \mu\text{m}$. An x-ray beam of less than $10 \mu\text{m}$ is thus required. Too small a beam size may

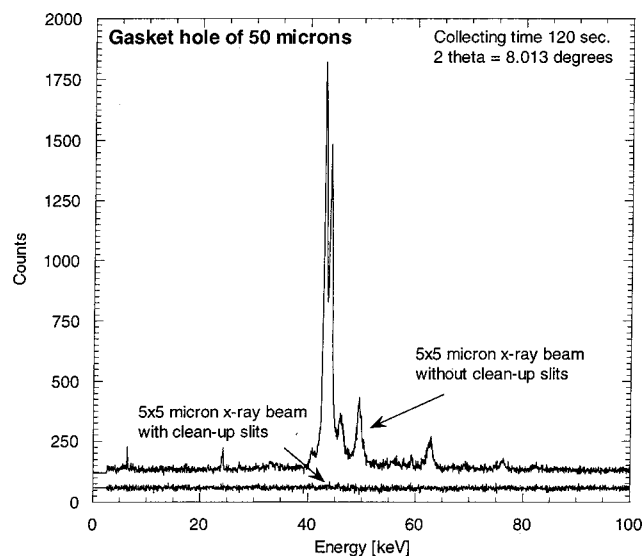


FIG. 12. Diffraction patterns of a stainless steel gasket with an empty hole of $50\ \mu\text{m}$. An x-ray beam with and without cleanup slits was located at the center of the hole. Gasket diffraction can be clearly observed with the x-ray beam without cleanup slits in place, while the diffraction was not seen when the cleanup slits were used.

cause other problems, however, such as insufficient statistics for powder diffraction. A beam of $3\text{--}10\ \mu\text{m}$ is found to be optimal. Two microbeam techniques are adopted: slits and focusing mirrors

X-ray beams of $3\text{--}10\ \mu\text{m}$ are collimated with a parallel slit system.³¹ The microbeam is further “cleaned” by another parallel slit system with slightly larger gaps (about $5\ \mu\text{m}$ larger). The so-called “cleanup” slits are essential to avoid beam broadening caused by edge effects from the primary slits. The effectiveness of the cleanup slits was tested by putting a stainless steel gasket with a hole $50\ \mu\text{m}$ in diameter on the sample stage. When a $5 \times 5\ \mu\text{m}^2$ x-ray beam was at the center of the empty hole without the cleanup slit, gasket diffraction could be clearly detected, whereas the gasket diffraction was eliminated with the cleanup slits in position (Fig. 12). The parallel slit system provides a well-collimated x-ray beam, but the total x-ray flux decreases rapidly with decreasing slit size.

For experiments in which the total flux is important, a microfocusing system consisting of two bent Kirkpatrick–Baez (KB) mirrors is used.³² Figure 13 shows the result of a sharp edge scan. A $70 \times 70\ \mu\text{m}^2$ white beam can be focused to $3\text{--}10\ \mu\text{m}$ at the FWHM with the focusing system. However, the full width at the 1% level could be over $30\ \mu\text{m}$. This “tail” may be cleaned by putting a slit system or pinhole very close to the sample. From Fig. 2, because of the laser heating optics, this distance cannot be less than $60\ \text{mm}$, resulting in the beam cleanliness being limited. Depending on the specific experiment, our system provides options of the slit system for cleanliness or the KB mirror system for flux.

C. Pressure calibrants

While temperatures can be measured by the spectral radiometry method, pressures were usually not measured di-

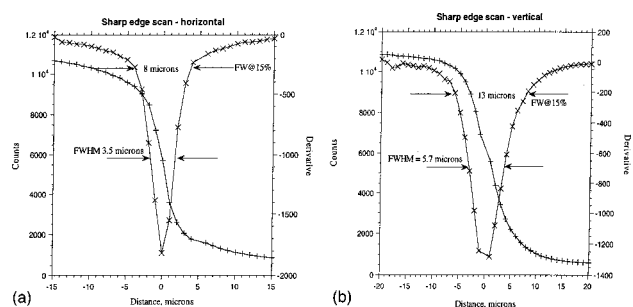


FIG. 13. Sharp edge scan measuring the x-ray beam size. A beam size of $3.5(\text{H}) \times 5.7(\text{V})\ \mu\text{m}$ at FWHM is measured. The KB mirror is used in the horizontal direction, while the vertical direction is controlled by a slit. We believe a beam size of $3\text{--}10\ \text{mm}$ is optimal in x-ray diffraction experiments with the LHDAC.

rectly at high temperature in the LHDAC until coupling of the LHDAC technique with the synchrotron.^{11,12} The effects of temperature on sample pressure include thermal pressure and the temperature dependence on the shear strength of materials. These effects could be different for various samples and for different loading configurations. Thus a calibrant should be thoroughly mixed with the sample, allowing observations of local temperature effects on pressure as well as on the effect of load. Such an internal standard should have (1) chemical inertness, (2) an available $P\text{--}V\text{--}T$ equation of state, (3) a simple x-ray diffraction pattern, and (4) no phase transition in the $P\text{--}T$ range of interest. At high temperature, alloy formation could occur between metal standards, which suggests that an inert metal–oxide (or silicate) pair is the best choice for experiments. Possible candidates include Au, Pt, Ag, NaCl, and MgO. Errors in determining the pressure in this way are limited to the accuracy of the standards.

D. X-ray measurements

In situ x-ray diffraction has been the primary analytical technique in the LHDAC.^{5,11,19} The key components for coupling of our laser heating system with the x-ray diffraction measurement are the x-ray transparent mirrors, such as beryllium and glassy carbon (m6 in Fig. 2). The mirror is coated with silver, providing reflectivity of $>98.5\%$ from the visible region to the infrared, including the laser wavelength, $1.053\ \mu\text{m}$. The beryllium mirror is transparent to x rays at energies greater than $5\ \text{keV}$, thus allowing x-ray diffraction measurements. For angle dispersive diffraction with an area detector, the beryllium mirror introduces diffraction lines and high background. The glassy carbon mirror is then used.

Polycrystalline x-ray diffraction is usually performed along the axis of the diamond cell with the incident and diffracted x rays passing through the diamond (axial diffraction). With the low- Z gasket technique (beryllium, boron), x-ray diffraction can be measured through the low- Z gasket, with the loading axis of the DAC perpendicular to the primary x-ray direction (radial diffraction).^{33,34} Radial diffraction provides crucial information on sample stress and strain. Coupling the laser heating system to the radial diffraction geometry is relatively straightforward because the optical paths can be arranged in the direction perpendicular to the x-ray beam and, therefore, the spatial limitations are relaxed.

This optical arrangement can be also applied to other x-ray techniques, such as x-ray spectroscopy. One caution should be taken when the x-ray beam passes through a gasket. In axial diffraction geometry, we just need a laser heating spot larger than the x-ray beam. If the x-ray beam is perpendicular to the laser beam path as in radial diffraction, then the radial diameter of the sample should be less than a focused laser beam size to avoid signals from any cold part of the sample along the x-ray path.

VII. DISCUSSION

A double-sided LHDAC system was developed and is operational at the GeoSoilEnviroCARS sector at the Advanced Photon Source. The laser heating system allows the generation of a large heating volume compared to the x-ray beam size, allowing *in situ* x-ray measurements at simultaneously ultrahigh pressures (to >160 GPa) and ultrahigh temperatures (to >4000 K). Typical heating areas 10–25 μm in diameter from both sides result in minimum temperature gradients in the sampling volume both radially and axially in the diamond anvil cell and minimal error arising from chromatic aberration in the temperature measurement. A feedback system permits steady heating of a DAC sample for minutes to hours. Temperatures can be controlled remotely by software. When combined with the x-ray microbeam (3–10 μm) technique, a temperature variation of less than 50 K can be achieved within the x-ray sampled region over a 10 min per 10 s. The LHDAC is the coupling of two parts: the laser beam and the heating object in the DAC. Proper sample configuration design and preparation, including effective use of insulation layers, are crucial for a successful experiment.

ACKNOWLEDGMENTS

Thanks are due to Yan-zhang Ma, Abby Kavner, Dan Shim, and M. Somayazulu for the help in constructing the system, to the DAC design team members (William Bassett, Tom Duffy, Dion Heinz, Rus Hemley, Ho-kwang Mao, and Li-chung Ming) for their continuous support. GSECARS's staff, Peter Eng, Paul Murray, Fred Sopron, Mike Jagger, Matt Newville, Nancy Lazarz, and T. Uchida provided invaluable support for this program. Jing Liu is thanked for detail drawings. Comments from an anonymous reviewer improved the article. This work was supported by NSF-Earth Science Instrumentation and Facilities, DOE-Geosciences, and the W. M. Keck Foundation.

¹L. C. Ming and W. A. Bassett, *Rev. Sci. Instrum.* **9**, 1115 (1974).

²H. K. Mao, T. Yagi, and P. M. Bell, *Year Book-Carnegie Inst. Washington* **76**, 502 (1977).

³R. Jeanloz and D. L. Heinz, *J. Phys. (Paris)* **45**, 83 (1984).

⁴R. Boehler, N. Von Bargen, and A. Chopelas, *J. Geophys. Res.* **95**, 21 (1990).

⁵G. Shen, H. K. Mao, R. J. Hemley, T. S. Duffy, and M. L. Rivers, *Geophys. Res. Lett.* **25**, 373 (1998).

⁶L. Liu, *Phys. Earth Planet Inter.* **11**, 289 (1976).

⁷R. Boehler, *Nature (London)* **363**, 534 (1993).

⁸E. Knittle and R. Jeanloz, *Science* **235**, 668 (1987).

⁹Q. Williams, R. Jeanloz, J. Bass, B. Svendsen, and T. J. Ahrens, *Science* **236**, 181 (1987).

¹⁰G. Shen, P. Lazor, and S. K. Saxena, *Phys. Chem. Miner.* **20**, 91 (1993).

¹¹G. Fiquet, D. Andrault, A. Dewaele, T. Charpin, M. Kunz, and D. Hausermann, *Phys. Earth Planet. Inter.* **105**, 21 (1998).

¹²S. Shim, T. S. Duffy, and G. Shen, *J. Geophys. Res.* **105**, 25955 (2000).

¹³G. Shen, M. L. Rivers, Y. Wang, and S. R. Sutton, in *Science and Technology of High Pressure*, Vol. 2, edited by M. H. Manghnani, W. J. Nellis, and M. F. Nicol (Universities Press, Hyderabad, India, 2000), pp. 1043–1046.

¹⁴D. L. Heinz and R. Jeanloz, in *High Pressure Researches in Mineral Physics*, edited by H. M. Manghnani and Y. Syono (AGU, Washington, DC, 1987), p. 113.

¹⁵D. L. Heinz, J. S. Sweeney, and P. Miller, *Rev. Sci. Instrum.* **62**, 1568 (1991).

¹⁶R. Boehler and A. Chopelas, in *High Pressure Research: Application to Earth and Planetary Sciences*, edited by Y. Syono and M. H. Manghnani (AGU, Washington, DC, 1992), p. 55.

¹⁷G. Shen, H. K. Mao, and R. J. Hemley, in *Advanced Materials'96—New Trends in High Pressure Research* (NIRIM, Tsukuba, Japan, 1996), p. 149.

¹⁸H. K. Mao, G. Shen, R. J. Hemley, and T. S. Duffy, in *Properties of Earth and Planetary Materials*, edited by M. H. Manghnani and T. Yagi (AGU, Washington, DC, 1998), p. 27.

¹⁹D. Andrault, G. Fiquet, M. Kunz, F. Visocekas, and D. Hausermann, *Science* **278**, 831 (1997).

²⁰C. S. Yoo, J. Akella, A. Compbell, H. K. Mao, and R. J. Hemley, *Science* **270**, 1473 (1995).

²¹D. L. Heinz and R. Jeanloz, *J. Geophys. Res.* **92**, 11437 (1987).

²²P. Lazor, G. Shen, and S. K. Saxena, *Phys. Chem. Miner.* **20**, 86 (1993).

²³From the web-page: <http://www.kosi.com/raman/applications/technotes/hsmimage.html>, a figure shows cross sections of images of an atomic line through a 10 μm slit generated with a quarter-meter *f*/4 Czerny–Turner spectrograph without prefiltering optics, and a Kaiser Optical Systems, Inc., axial transmissive spectrograph *f*/1.8. The axial transmissive spectrograph broadened the image of the slit by only 4 μm , while the quarter-meter Czerny–Turner broadened the image by 30 μm .

²⁴R. Boehler, *Geophys. Res. Lett.* **13**, 1153 (1986).

²⁵J. S. Sweeney and D. L. Heinz, in Ref. 18, p. 197.

²⁶F. Cabannes, *J. Phys. (Paris)* **28**, 235 (1967).

²⁷R. Boehler, G. Fiquet, H.-J. Reichmann, and A. Zerr, *HASYLAB, 1993*, Vol. 1993, p. 649.

²⁸R. Boehler, M. Ross, and D. B. Boercker, *Phys. Rev. Lett.* **78**, 4589 (1997).

²⁹S. D. Jacobs, K. A. Cerqua, K. L. Marshall, A. Schmid, M. J. Guedalben, and K. J. Skerrett, *J. Opt. Soc. Am. B* **5**, 1962 (1988).

³⁰G. Shen, T. S. Duffy, M. L. Rivers, P. J. Eng, S. R. Sutton, and Y. Wang, in *Proceedings of International Conference on High Pressure Science and Technology*, Vol. 7, edited by M. Nakahara (Nakanishi Printing, Kyoto, 1997), p. 1529–1531.

³¹H. K. Mao and R. J. Hemley, *High Press. Res.* **14**, 257 (1996).

³²P. J. Eng, M. Newville, M. L. Rivers, and S. R. Sutton, *Proc. SPIE* **3449**, 145 (1998).

³³K. Mao, J. Shu, G. Shen, R. J. Hemley, B. Li, and A. K. Singh, *Nature (London)* **396**, 741 (1998).

³⁴S. Duffy, G. Shen, D. L. Heinz, Y. Ma, J. Shu, H. K. Mao, R. J. Hemley, and A. K. Singh, *Phys. Rev. B* **60**, 15063 (1999).